PHYSICAL REVIEW E **86**, 045202(R) (2012)

Two- and three-dimensional standing waves in a reaction-diffusion system

Tamás Bánsági, Jr.,[1] Vladimir K. Vanag,[1,2] and Irving R. Epstein[1,*]
[1]*Department of Chemistry, Brandeis University, Mail Stop 015, Waltham, Massachusetts 02454-9110, USA*
[2]*Immanuel Kant Baltic Federal University, A. Nevskogo 14, Kaliningrad 236041, Russia*
(Received 17 April 2012; published 15 October 2012)

We observe standing waves of chemical concentration in thin layers [quasi-two-dimensional (2D)] and capillaries [three-dimensional (3D)] containing the aqueous Belousov-Zhabotinsky reaction in a reverse microemulsion stabilized by the ionic surfactant sodium bis-2-ethylhexyl sulfosuccinate (AOT) and with cyclo-octane as the continuous phase. The 3D structures are oscillatory lamellae or square-packed cylinders at high and low volume fractions, respectively, of aqueous droplets. These patterns correspond to oscillatory labyrinthine stripes and square-packed spots in the 2D configuration. Computer simulations, as well as observations in *E. coli*, give qualitative agreement with the observed patterns and suggest that, in contrast to Turing patterns, the structures are sensitive to the size and shape of the system.

DOI: 10.1103/PhysRevE.86.045202 PACS number(s): 82.40.Bj, 82.40.Ck, 82.20.Wt, 82.33.Nq

Waves and patterns in physical, chemical, and biological systems have fascinated scientists for centuries [1,2]. Their appeal can be attributed not only to the importance of these phenomena in objects ranging from microorganisms to galaxies, but also to the beauty of many natural patterns and the intellectual challenge of explaining their origin. Among pattern-forming systems, reaction-diffusion systems are particularly attractive by virtue of their versatility, their experimental accessibility, and their relevance to biological patterns.

Standing waves (SWs) in reaction-diffusion systems were first reported in the heterogeneous catalytic oxidation of carbon monoxide on a platinum surface [3,4]. The first experimental observations of several phenomena associated with wave instability—standing waves, antiwaves, and packet waves—in homogeneous chemical systems [5–7] were made in the BZ-AOT system [8]. Here, BZ refers to the Belousov-Zhabotinsky (BZ) oscillatory chemical reaction [9,10], and AOT is the common name for the anionic surfactant sodium bis-2-ethylhexyl sulfosuccinate. The system consists of a reverse microemulsion, in which the polar reactants of the BZ reaction reside in water nanodroplets of the microemulsion suspended in a continuous oil phase [11]. An AOT microemulsion can be characterized by two parameters: the mean radius of the water nanodroplets R_w and their concentration c_d, or by the equivalent, more convenient parameters $\omega = [H_2O]/[AOT]$, where $[H_2O]$ and [AOT] are the bulk concentrations of water and surfactant, respectively, $R_w/\text{nm} \approx 0.17\omega$ [12], and the volume fraction of droplets φ_d.[1]

The above patterns were obtained in a quasi-two-dimensional (2D) geometry, the thickness of which was less than $\lambda/2$, where λ is the characteristic wavelength of the pattern. In biological systems, however, many patterns are three dimensional (3D). The geometry and stability of 3D dissipative patterns are not as well characterized as their 2D counterparts. The first experimental observations of 3D Turing patterns, for example, were made only in 2011 [13], though earlier theoretical studies had predicted their existence [14]. The experiments showed that the geometry of 3D Turing patterns may be quite different from that of 2D structures. For example, hexagonally packed cylinders, curved surfaces, and parallel planes (lamellar structures) were observed in 3D.

In this Rapid Communication, we investigate 2D and 3D *standing wave patterns* emerging from the wave instability in the BZ-AOT system. Standing waves differ from Turing patterns in that the former are temporally as well as spatially periodic, arise via a wave rather than a Turing bifurcation, and are sensitive to the size and shape of the system primarily due to reflection of packet waves that originated from a perturbation.

2D BZ-AOT reverse microemulsions with $\omega = 12.35$ and a chosen droplet fraction φ_d in the range 0.39–0.55 were prepared using a procedure described elsewhere [7]. For the 3D experiments, the reaction mixture was transferred by capillary action 50–60 mm into a circular quartz capillary, which was subsequently sealed at one end and submerged in a rectangular cuvette containing cyclo-octane. Cyclo-octane was employed as the bulk oil phase instead of octane, which is more commonly used in BZ-AOT microemulsions, because the refractive index of cyclo-octane is quite close to that of quartz glass. This index-matching enabled us to minimize undesired effects of refraction on the image quality. Both the 2D and 3D samples were illuminated through 510-nm interference filters and observed in transmitted light through long focal length objectives equipped with charge-coupled device cameras. Visualization of the 3D reaction medium was implemented by optical tomography. This method, previously employed to study scroll waves [15], scroll rings [16], and Turing patterns [13], relies on a series of projections of a reaction medium recorded as transmittance images during a full rotation of the sample. Our image data typically consisted of 100 snapshots of the rotating capillary acquired at a frame rate of 25 frames per second. The SWs had a typical period of 50–60 s, about 14 times longer than the rotation cycle of the sample (4 s). Consequently, the patterns can be considered nearly stationary within a complete rotation of the reaction medium. Concentration fields of the

*epstein@brandeis.edu

[1] $\varphi_d = \varphi_w + \varphi_{AOT}$; $\varphi_d + \varphi_{oil} = 1$; $c_d = \varphi_w/(N_A V_{dw})$, $V_{dw} = 4\pi R_w^3/3$; $\varphi_w = V_w/V_0$, where V_0 is the total volume of microemulsion and V_w is the volume of added water, N_A is Avogadro's number, $\varphi_{AOT} = [AOT]M_{AOT}/d_{AOT}$, $M_{AOT} = 444.5$ g/mol, $d_{AOT} = 1.151$ g/mL; $\varphi_d \cong \varphi_w(1 + 21.6/\omega)$; $\varphi_d \cong [H_2O]/55.5 + [AOT]/2.59$.

oxidized form of the catalyst, ferriin, were reconstructed by computing the inverse Radon transform [17] of the filtered image data. All experiments were carried out at room temperature.

In both 2D and 3D, SWs emerged directly from the homogeneous oxidized state about 10 min after the start of the reaction. A similar induction period preceded bulk relaxation oscillations in the continuously stirred batch system at the same composition. Once fully developed, the SWs exhibited striking similarities to those resulting from interference between oppositely traveling waves or those produced when a wave train propagates in a medium that moves in the opposite direction. The antinodes had relatively low amplitude compared to the Turing patterns or traveling waves found previously in the BZ-AOT system [7]. Since our system was closed, any patterns observed were necessarily transient. To our knowledge, an experimental configuration remains to be developed that allows study of pattern formation in a true open system. The SWs persisted for about 20 min, i.e., 20 or more oscillatory cycles, before giving way to either trigger waves or packet waves, depending on the initial conditions, from which we infer that the SWs would be stable under open conditions. For initial concentrations $[H_2SO_4]_0 = 0.25$ mol/L, $[NaBrO_3]_0 = 0.3$ mol/L, $[\text{ferroin}]_0 = 0.4$ mmol/L, we observed transitions to trigger waves for initial malonic acid (MA) concentrations in the range 0.275–0.325 mol/L and to packet waves for $[MA]_0 \approx 0.350$ mol/L. Note that large-amplitude trigger waves can arise in excitable media, while packet waves and SW require a wave instability.

In 2D, two types of SWs developed: labyrinthine stripes [Fig. 1(a)] and spots on a square lattice [Fig. 2(a)]. At the concentrations of BZ reactants employed in our experiments, the droplet fraction determined which type of pattern formed. At higher φ_d, oscillatory stripes evolved, whereas lower droplet fractions favored oscillatory spots. The critical value of φ_d separating the two domains depended on the initial BZ concentrations. Decreasing $[MA]_0$, for example, resulted in a lower droplet fraction dividing the stripe and spot regimes. Space-time plots show the spatiotemporal behavior of the two types of SWs. In the case of stripes, the pattern dynamics is presented along a cross section perpendicular to the lines of nodes and antinodes [Fig. 1(b)]. For spots, we chose two cross

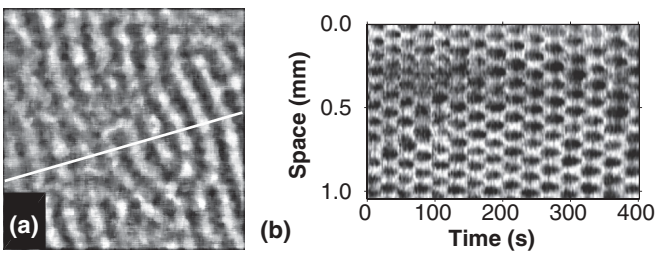

FIG. 1. Standing waves composed of stripes in a thin layer of the BZ-AOT reaction medium. (a) was taken 1080 s after the experiment was started. Space-time plot (b) was computed along the cross section indicated with a white line in (a). Initial concentrations: $[MA]_0 = 0.3$ mol/L, $[H_2SO_4]_0 = 0.25$ mol/L, $[NaBrO_3]_0 = 0.3$ mol/L, $[\text{ferroin}]_0 = 0.4$ mmol/L; $\omega = 12.35$, $\varphi_d = 0.54$. Field of view in (a): 1×1 mm^2. Light (dark) areas represent lower (higher) concentrations of ferroin.

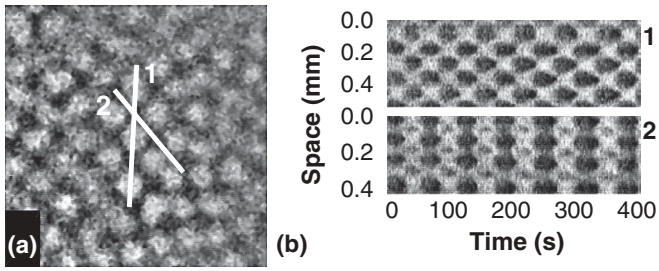

FIG. 2. SWs consisting of spots in a quasi-two-dimensional layer of the BZ-AOT reaction medium. Space-time plots (b) represent the cross sections marked with white lines in (a). (a) was taken 968 s after the reaction was started, which corresponds to $t = 318$ s in the space-time plots. Concentrations as in Fig. 1, $\varphi_d = 0.44$. Frame size in (a) $= 1 \times 1$ mm^2.

sections that cross at a 45° angle. The first space-time plot [Fig. 2(b)] shows behavior similar to that of stripes, whereas the second reveals the local dynamics at the intersection of nodes. The space-time plots demonstrate that the oscillatory behavior of the antinodes is characterized by expansion of the oxidized domains, followed shortly by a transition to the reduced state, which begins in the middle of each stripe, or in the center of each spot, and propagates outward. The half cycle ends when the area of the reduced antinode reaches the size of the oxidized antinode it evolved out of. The process then continues in a similar fashion, starting with the newly formed oxidized domains, until the original configuration is restored, marking the beginning of a new cycle.

In 3D, the two major types of SWs we found were oscillatory lamellae and cylinders. We also observed oscillatory spots at $\varphi_d \approx 0.35$, but the lifetime of this pattern was considerably shorter than that of the other two. Transmittance images of patterns in capillaries with inner diameters greater than 0.4 mm had very low contrast due to the small amplitude of the SWs. Tomographic reconstruction of patterns above that width was therefore greatly hindered. Visual observation revealed that in wide capillaries both robust patterns tended to take on irregular configurations. Decreasing the inner diameter enhanced contrast, allowing for adequate visualization, and resulted in more symmetric SWs. Similar to 2D, where the droplet fraction determined which type of pattern formed, we found that at higher φ_d lamellae emerged, whereas square-packed oscillatory cylinders arose when φ_d was lower. Parallel experiments showed that the same chemical composition typically produced oscillatory lamellae in 3D and stripes in 2D, or oscillatory cylinders and spots in the capillary and in the thin layer, respectively. Lateral views of 3D standing waves with a π phase shift are shown in Figs. 3(a), 3(c), 4(a), and 4(c). Despite the low contrast, vertical bright bands can be discerned in all projections. These observations are insufficient to determine the spatial geometry of the patterns. By using optical tomography, we were able to reconstruct the structures and hence identify the two robust types of SWs in 3D as oscillatory lamellae [Figs. 3(b) and 3(d)] and cylinders [Figs. 4(b) and 4(d)].

Turing patterns require that an inhibitor species diffuse significantly more rapidly than an activator species. The necessary conditions for wave instability are not as easily characterized.

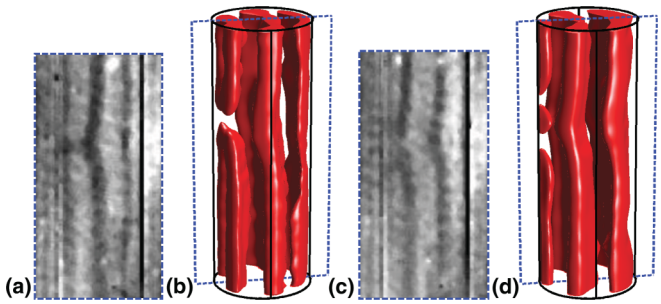

FIG. 3. (Color online) Lamellar standing waves in the three-dimensional BZ-AOT system. 2D projections (a), (c) were taken as transmittance images through the planes indicated with dashed lines in (b), (d). Concentrations as in Fig. 1, $\varphi_d = 0.46$. Time elapsed between (a), (b) and (c), (d): 26 s. Inner diameter of capillary: 0.3 mm; height of cross sections: 0.8 mm.

In general, it is possible to obtain wave instability by having either a fast-diffusing activator [5] or a fast-diffusing inhibitor in a model with three or more variables.

We examined a four-variable model [18] with variables x (activator, $HBrO_2$), y (inhibitor, Br^-), and z (oxidized form of the catalyst) in the aqueous phase, and u, an inhibitor (Br_2), in the oil phase:

$$\partial x/\partial\tau = [-xy + qy - x^2 + x(1 - z/z_m)/(1 - z/z_m + \mu)]/\varepsilon_1 + D_x\nabla^2 x, \quad (1)$$

$$\partial y/\partial\tau = (-3xy - 2qy - x^2/2 + 2u + fz)/\varepsilon_2 + D_y\nabla^2 y, \quad (2)$$

$$\partial z/\partial\tau = x(1 - z/z_m)/(1 - z/z_m + \mu) - z + D_z\nabla^2 z, \quad (3)$$

$$\partial u/\partial\tau = (xy + qy/2 + x^2/4 - u)/\varepsilon_3 + D_u\nabla^2 u, \quad (4)$$

where $D_x, D_y, D_z \ll D_u$.

In our simulations we used the software package FLEXPDE, version 6 [19]. The model, which is derived from a detailed seven-variable, 12-step description of the BZ chemistry in the Supplemental Material [20], incorporates the chemistry of the BZ reaction and the differential diffusion in the aqueous and oil phases.

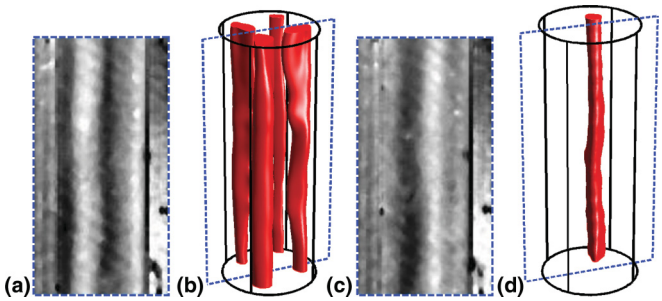

FIG. 4. (Color online) Square-packed cylinders as 3D standing waves in the BZ-AOT reaction. Two-dimensional projections (a), (c) were taken through the planes marked with dashed lines in (b), (d). Concentrations as in Fig. 1, $\varphi_d = 0.39$. (a), (c) and corresponding 3D structures (b), (d) are 28 s apart. Inner diameter of capillary: 0.3 mm; height of cross sections: 0.8 mm.

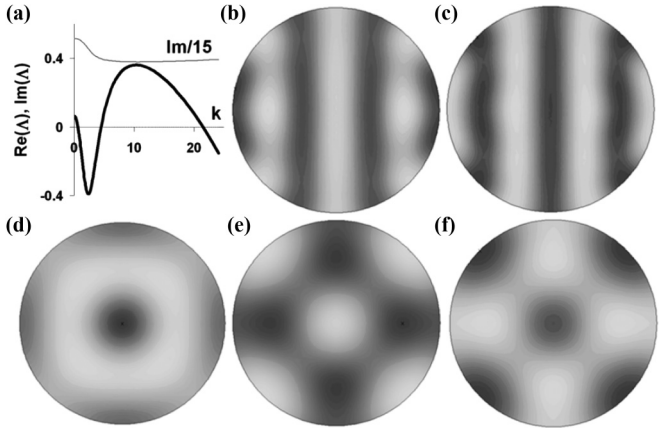

FIG. 5. (a) Dispersion curves of model (1)–(4) showing wave instability. Re(Λ) and Im(Λ) are real and imaginary parts, respectively, of the eigenvalue with the largest real part, Λ, in the linearized model. Dimensionless parameters (corresponding to experimental concentrations): $D_x/D_u = D_y/D_u = 0.0015$, $D_z/D_u = 0.0012$, $D_u = 1$, $q = 4.5 \times 10^{-4}$, $f = 1.05$, $\varepsilon_1 = 0.016$, $\varepsilon_2 = 4.2 \times 10^{-4}$, $\varepsilon_3 = 0.1$, $\mu = 0.03$; $z_m = 0.006$. (b) and (c) are two antiphase snapshots of simulated striped standing wave patterns; diameter $= 3\lambda$. (d)–(f) are three snapshots of simulated spotlike SW patterns with square symmetry taken at different phases of a full oscillatory cycle; diameter $= 2\lambda$. The condition $v_g \cong 0$, which is necessary for such patterns to appear, is fulfilled over a broad range of parameters.

We performed linear stability analysis of model (1)–(4) to obtain sets of parameters that gave dispersion curves typical for wave instability as shown in Fig. 5(a). Curve "Re," the real part of eigenvalue Λ, has a positive maximum at a wave number k_{max}, where curve "Im/15," the imaginary part of Λ, shows that Λ is complex. The values $2\pi/k_{max}$ and $2\pi/\mathrm{Im}(\Lambda)$ at $k = k_{max}$ are equal to the characteristic wavelength λ and period of oscillation of the SWs, respectively. The positive value of Re(Λ) at $k = 0$ implies that we have Hopf instability (bulk oscillations also seen in the parallel, continuously stirred batch experiments for chemical compositions producing standing waves) as well at this set of parameters.

To find parameters that favor spotlike patterns (as in Fig. 2) or stripelike patterns (as in Fig. 1), it is necessary to analyze amplitude equations [21] corresponding to model (1)–(4). At present, such equations are unavailable. In the very limited literature on amplitude equations for wave instability in 2D (e.g., coupled complex Ginzburg-Landau equations) [22–24], the differentiation between spotlike and stripelike SW patterns is not discussed. We are unaware of any literature on amplitude equations for 3D wave instability in reaction-diffusion systems.

Our calculations, which provide a qualitative understanding of the observed phenomena, suggest that the symmetry of the patterns strongly depends on the shape of the system boundaries, the symmetry of the initial perturbation of the steady state, and the group velocity of waves, $v_g = d\ \mathrm{Im}(\Lambda)/dk$. Any initial perturbation results in a packet of traveling waves that propagate with velocity v_g. The value of v_g depends on the diffusion coefficients, which in turn depend on the microemulsion droplet fraction φ_d. If $v_g \cong 0$, many patterns of different symmetries are stable for hundreds of oscillation

periods. If v_g differs significantly from zero and the initial perturbation lacks azimuthal symmetry, a SW pattern with square symmetry, as in Fig. 4, emerges [Figs. 5(d)–5(f)] after several reflections from the boundaries. For example, an initial perturbation consisting of stripes with characteristic wavelength λ, as in Fig. 3, gives stable striped SWs in our simulations [Figs. 5(b) and 5(c)]. This observation suggests why we observed stripe or lamellar patterns at one φ_d and spotlike patterns with square symmetry at another φ_d. However, more careful theoretical investigation, ideally using amplitude equations, is necessary.

Three-dimensional SWs have been studied in unreactive optical, mechanical, or acoustic media [21,25–27], but observations in chemical systems are lacking. The SWs reported here in the BZ-AOT reaction and those seen in physical systems have similar features, including the temporal dynamics of the antinodes and their spatial symmetry, i.e., stripes or square arrangements of spots. The two types of SWs, however, appear to differ in the dynamics of their nodes. In the reactive microemulsion, where the local oscillations are strongly nonsinusoidal, the "nodes" have nonzero amplitude. Moreover, the oscillation frequency of the nodes is twice that of the antinodes, which is apparent from the space-time plots [Figs. 1(b) and 2(b), top], if one looks at the time evolution in the narrow regions halfway between the antinodes.

Similar behavior was observed in *Escherichia coli* cells when the distribution of the membrane ATPase protein, MinD, was monitored during cell growth [28]. When the bacteria reached a certain length, the erratic switching of the distribution of the protein between the two halves of a cell became regular in time. Periodicity, required for positioning the division plane, was maintained until the bacteria extended to a critical length, when cell division commenced. The time evolution of two neighboring antinodes in our quasi-2D experiments greatly resembles this periodic dynamics captured in space-time plots taken along the long axes of the bacteria.

As the *E. coli* example demonstrates, the size of a system can affect the pattern within it, especially when its dimensions are only a few times the characteristic wavelength of the pattern. Numerical simulations suggest that the symmetry of patterns can also be influenced by the size and geometry of the pattern-forming system [29,30]. Consequently, the reason for the weak stability of spots in 3D may lie in the inadequate size and/or geometry of our reaction vessels. Other media, such as hydrogels, in which BZ patterns have recently been found [30], may merit investigation. Also, this sensitivity of patterns to the shape and size of the media they evolve in makes it likely that SW with symmetries different from those found in this study can occur. These ordered configurations may include oscillatory concentric cylinders and spheres of lamellae, spots in a body-centered cubic lattice, and patterns with various rotational symmetries.

T.B. was supported by Grant No. 2008241 from the United States–Israel Binational Science Foundation. This work was supported in part by grants from the Army Research Office (W911NF-09-1-0496) and the National Science Foundation (CHE-1012428).

[1] M. Cross and H. Greenside, *Pattern Formation and Dynamics in Nonequilibrium Systems* (Cambridge University Press, Cambridge, UK, 2009).
[2] R. B. Hoyle, *Pattern Formation. An Introduction to Methods* (Cambridge University Press, Cambridge, UK, 2006).
[3] A. von Oertzen, H. H. Rotermund, A. S. Mikhailov, and G. Ertl, J. Phys. Chem. B **104**, 3155 (2000).
[4] S. Jakubith, H. H. Rotermund, W. Engel, A. von Oertzen, and G. Ertl, Phys. Rev. Lett. **65**, 3013 (1990).
[5] V. K. Vanag and I. R. Epstein, Phys. Rev. Lett. **88**, 088303 (2002).
[6] V. K. Vanag and I. R. Epstein, Science **294**, 835 (2001).
[7] V. K. Vanag and I. R. Epstein, Phys. Rev. Lett. **87**, 228301 (2001).
[8] V. K. Vanag and D. V. Boulanov, J. Phys. Chem. **98**, 1449 (1994).
[9] B. P. Belousov, *Sbornik Referatov po Radiatsionni Meditsine* (Medgiz, Moscow, 1958), p. 145.
[10] A. M. Zhabotinsky, Dokl. Akad. Nauk SSSR **157**, 392 (1964).
[11] T. K. De and A. Maitra, Adv. Colloid Interface Sci. **59**, 95 (1995).
[12] M. Kotlarchyk, S. H. Chen, and J. S. Huang, J. Phys. Chem. **86**, 3273 (1982).
[13] T. Bánsági, V. K. Vanag, and I. R. Epstein, Science **331**, 1309 (2011).
[14] A. De Wit, G. Dewel, P. Borckmans, and D. Walgraef, Physica D **61**, 289 (1992).
[15] A. T. Winfree, S. Caudle, G. Chen, P. McGuire, and Z. Szilagyi, Chaos **6**, 617 (1996).
[16] T. Bánsági and O. Steinbock, Phys. Rev. Lett. **97**, 198301 (2006).
[17] A. S. Kak and M. Slaney, *Principles of Computerized Tomographic Imaging* (IEEE, New York, 1988).
[18] V. K. Vanag and I. R. Epstein, J. Chem. Phys. **131**, 104512 (2009).
[19] http://www.pdesolutions.com, (2011).
[20] See Supplemental Material at http://link.aps.org/supplemental/10.1103/PhysRevE.86.045202 for a derivation of the four-variable model used here from the full 12-variable model.
[21] I. S. Aranson and L. S. Tsimring, Physica A **249**, 103 (1998).
[22] H. Sakaguchi, Phys. Scr., T **67**, 148 (1996).
[23] H. Levine and X. Q. Zou, Phys. Rev. E **48**, 50 (1993).
[24] M. Ipsen and P. G. Sorensen, Phys. Rev. Lett. **84**, 2389 (2000).
[25] T. H. Lu, Y. C. Lin, Y. F. Chen, and K. F. Huang, Phys. Rev. Lett. **101**, 233901 (2008).
[26] S. Kamol, P. Limsuwan, and W. Onreabroy, Am. J. Phys. **78**, 492 (2010).
[27] N. Allalou, M. Debiane, and C. Kharif, Eur. J. Mech. B Fluids **30**, 371 (2011).
[28] E. Fischer-Friedrich, G. Meacci, J. Lutkenhaus, H. Chate, and K. Kruse, Proc. Natl. Acad. Sci. USA **107**, 6134 (2010).
[29] M. Dolnik, A. B. Rovinsky, A. M. Zhabotinsky, and I. R. Epstein, J. Phys. Chem. A **103**, 38 (1999).
[30] R. A. Barrio, P. K. Maini, J. L. Aragon, and M. Torres, Physica D **168**, 61 (2002).